PHYSICAL REVIEW D VOLUME 25, NUMBER 3 1 FEBRUARY 1982

Precise measurement of the asymmetry parameter in the decay $\Xi^0 \to \Lambda\pi^0$

R. Handler, R. Grobel, L. Pondrom, M. Sheaff, and C. Wilkinson
Department of Physics, University of Wisconsin, Madison, Wisconsin 53706

P. T. Cox, J. Dworkin, and O. E. Overseth
Department of Physics, University of Michigan, Ann Arbor, Michigan 48109

K. Heller
School of Physics, University of Minnesota, Minneapolis, Minnesota 55455

T. Devlin, L. Deck, K. B. Luk, R. Rameika, and P. Skubic
Department of Physics, Rutgers, The State University, Piscataway, New Jersey 08854

G. Bunce
Accelerator Division, Brookhaven National Laboratory, Upton, New York 11973
(Received 23 January 1981; revised manuscript received 20 August 1981)

The Λ helicity has been measured in a fully reconstructed sample of 3.0×10^5 $\Xi^0\to\Lambda\pi^0$ decays. The product $\alpha_\Lambda\alpha_{\Xi^0}$ was found to be -0.260 ± 0.006, or $\alpha_{\Xi^0}=-0.405\pm0.011$.

INTRODUCTION

Renewed interest in the nonleptonic weak decays of hadrons has been motivated by quantum chromodynamics. If the basic quark flavor transformation is presumed to be understood from the Weinberg-Salam theory of weak interactions,[1] then actual hadron decays $B\to B'\pi$ should be described by QCD radiative corrections to this fundamental quark transition.[2] A comparison of the measured amplitudes for various decays can help determine the nature and importance of these corrections. This paper presents the most precise measurement of the asymmetry parameter α_{Ξ^0} for the decay $\Xi^0\to\Lambda\pi^0$, from which a new value for the ratio of P-wave to S-wave amplitudes in this process is obtained.

EXPERIMENTAL TECHNIQUE

The Fermilab neutral-hyperon beam used for this experiment has been described previously.[3] The configuration is shown in plan and elevation view in Fig. 1. The hyperons were produced by 400-GeV protons which struck a $\frac{1}{2}$-interaction-length metal target, usually beryllium. The neutral beam contained Λ and Ξ^0 hyperons roughly in the ratio 50 to one. The production angle could be varied between 0 and 10 mrad by leaving the neutral beam line fixed and by deflecting the proton beam in the vertical plane with the magnet $M1$ in Fig. 1. A previous measurement of α_{Ξ^0} using this beam and an earlier version of the apparatus has been reported.[4] The two experiments had many features in common, since both the apparatus and the data analysis were basically the same, although the present result is based on 50 times as many Ξ^0-decay events (3.0×10^5), and differed from its predecessor in several other ways as well. All of the Ξ^0 hyperons analyzed in Ref. 4 were produced at 0 mrad, where the absolute yield was the highest, but the Ξ^0/Λ ratio was least favorable. Only 6% of the present data sample was taken at 0 mrad. Both γ rays from π^0 decay had to pass through the aperture of the analyzing magnet $M3$ and convert in the lead-glass array at the back of the apparatus to satisfy the event criteria used in Ref. (4). This category was augmented in this experiment by the addition of scintillator-lead-MWPC (multiwire proportional chamber) assemblies above and below the $M3$ aperture, as shown in Fig. 1(b). Decays $\pi^0\to\gamma\gamma$ where one γ ray struck the lead glass and one converted in the scintillator-lead-MWPC detectors were accepted, which roughly doubled the π^0 detection efficiency. The material in and near the neutral beam was held to a minimum to reduce spurious interactions

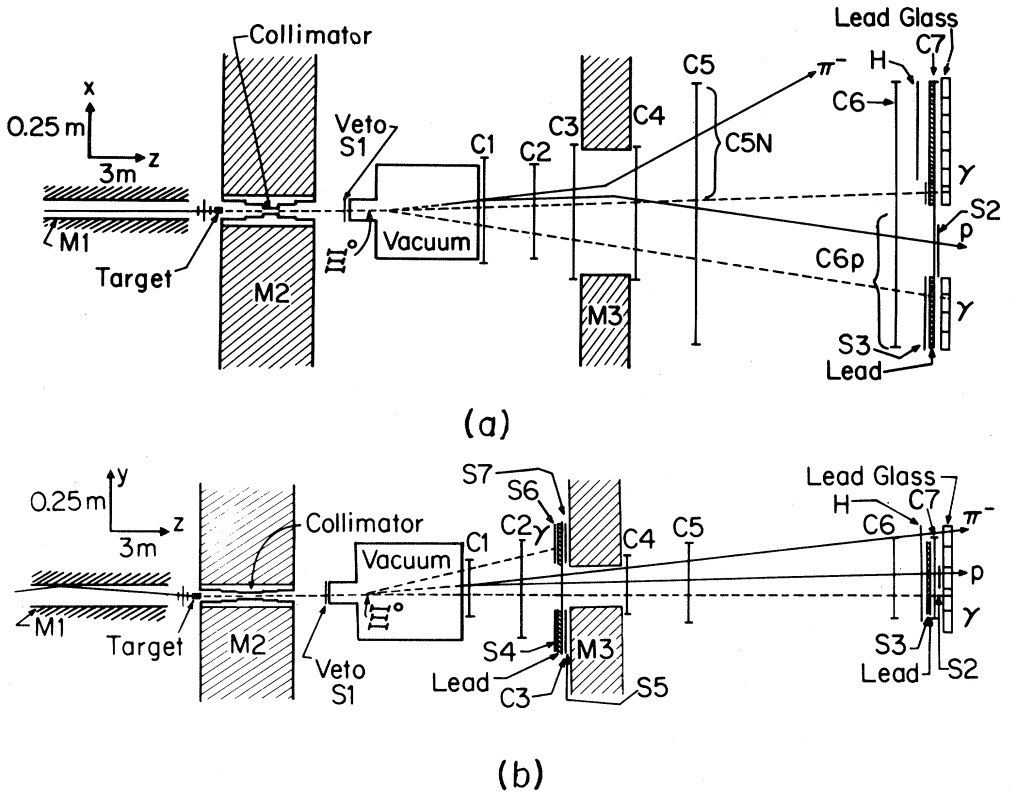

FIG. 1. The apparatus used in the present experiment shown in plan view in (a) and in elevation view in (b). The transverse scale is distorted relative to the longitudinal scale in each case. Two different decay events $\Xi^0 \rightarrow \Lambda\pi^0$, $\Lambda \rightarrow p\pi^-$, $\pi^0 \rightarrow \gamma\gamma$ are sketched in, a type $G2$ in (a) where both γ's strike the glass, and a type $G1$ in (b) where one γ hits chamber $C3$. The differences between this setup and the one described in Ref. 4 are the pion hodoscope H, the detectors on the face of $M3$, and the use of electronic cluster logic on the lead-glass array which improved the selection of Ξ^0-decay events at the trigger level. In addition, the magnet $M1$ was added to vary the production angle.

which complicated the γ-ray-detection process. The array of lead-glass shower-counter blocks—70 blocks each 100 mm × 100 mm × 384 mm (12 radiation lengths)—is shown in the plane normal to the neutral-beam direction in Fig. 2. It was essentially the same in the two experiments. The blocks were arranged in a rectangle five blocks high and 15 blocks wide. The staggered pattern, like bricks in a wall, decreased the number of nearest neighbors to a given block from eight to six, which simplified the cluster logic module. This fast electronic device, to be described below, detected individual γ-ray showers in the lead glass and improved the $\Xi^0 \rightarrow \Lambda\pi^0$ trigger efficiency.

The study of the decay sequence $\Xi^0 \rightarrow \Lambda\pi^0$, $\Lambda \rightarrow p\pi^-$, $\pi^0 \rightarrow \gamma\gamma$ in the neutral hyperon beam was complicated by the fact that beam Λ's could lead to false triggers from $\Lambda \rightarrow p\pi^-$ in association with random "showers" in the γ-ray detectors; and by the fact that the bending power of the $M3$ magnet was not sufficient to prevent charged particles

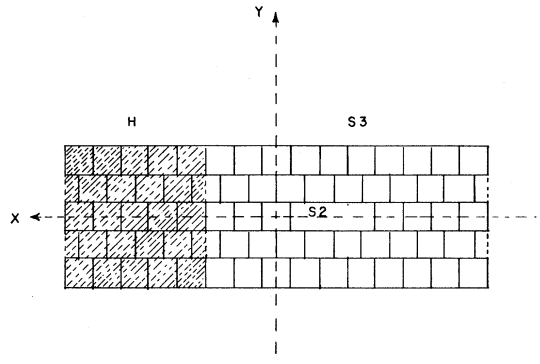

FIG. 2. The lead-glass array viewed along the neutral-beam line. The 70 blocks were each 10 cm × 10 cm × 38 cm lead glass with a radiation length of 3.2 cm. The shaded area to the left was covered by the pion hodoscope, consisting of five 10-cm-wide horizontal scintillator strips and ten 5-cm-wide vertical strips. The rest of the area was covered by the veto counter $S3$ except for the hole, which was covered by the separate proton counter $S2$.

from Λ decay from hitting the lead glass. Since a lead-glass block was about $\frac{1}{2}$ interaction length deep, many of these energetic hadrons could produce clusters in the array which would obscure the γ-ray detection. All of the protons from Λ decay would hit three lead-glass blocks immediately to one side of the neutral beam in the horizontal plane. To avoid problems from hadronic interactions, these three blocks were physically removed from the array, as shown in Fig. 2. The block in the neutral beam was recessed to prevent interactions in that block from spreading to its neighbors. Negative pions would hit the glass over a fairly broad area on the side opposite the protons. The large number of blocks involved precluded physical removal, so another solution was found. A hodoscope H with horizontal and vertical counters was used to determine the pion coordinates, and thus the coordinates of the subsequent hadronic shower in the lead glass. If a cluster occurred centered on these coordinates it was removed electronically from the on-line cluster logic, so that it did not count as a γ-ray candidate.

The setup behind the last MWPC on the $\Lambda \rightarrow p\pi^-$ spectrometer, $C6$, shown in Fig. 1, consisted of the pion hodoscope, a veto counter $S3$ covering the glass on the side opposite the hodoscope H, a 2-radiation-length-thick sheet of lead, another MWPC $C7$ used to measure γ-ray coordinates, and a proton coincidence counter $S2$ before the lead glass itself. The active area of $C7$ (1.28 m $\times$ 0.38 m) was centered on the lead glass, and the lead sheet immediately upstream of it was the same size. Holes 30 cm wide $\times$ 10 cm high were cut in the $S3$ veto and the lead sheet and were centered on the missing lead-glass blocks. The scintillator $S2$, which counted Λ-decay protons, was the same size as the hole and centered on it.

The lead-glass array was periodically calibrated with e^+e^- pairs made in the neutral beam and momentum analyzed by the spectrometer. The gains of individual lead-glass counters were monitored by pulsing four argon flash lamps, each of which was connected to a set of lead-glass blocks by fiber optics. In addition, the $\Xi^0 \rightarrow \Lambda\pi^0$ events themselves served as a continual gain check, because a one-constraint fit to the decay hypothesis could be made without using the γ-ray-energy information at all. The gains drifted typically less than 10% throughout the course of the experiment. The average position resolution of the array was ± 2.4 cm, which was reduced to ± 0.5 cm for those γ rays—about 75% of the total detected in the lead glass—which converted in the lead sheet just upstream of $C7$. The half width of the π^0 mass for those events with both γ's detected in the lead glass was primarily determined by the energy resolution, and was ± 30 MeV/c^2.

The pulse height from the phototube attached to each lead-glass block was compared with all of its neighbors to determine the number of separate clusters. This determination was performed over the entire lead-glass array in parallel by using a matrix of fast emitter-coupled-logic (ECL) comparators. Figure 3 shows a schematic diagram of the concept. The block C_n in the third row of the array had nearest neighbors C_{n-1} and C_{n+1} on the same row, B_n and B_{n-1} on the row above, and D_n and D_{n+1} on the row below. A fast comparison was made of C_n with the six other signals. If C_n was the largest pulse, was greater than a threshold minimum (about 1 GeV energy deposited in that block), and was not caused by an entering pion, then a one-cluster level was added to the output

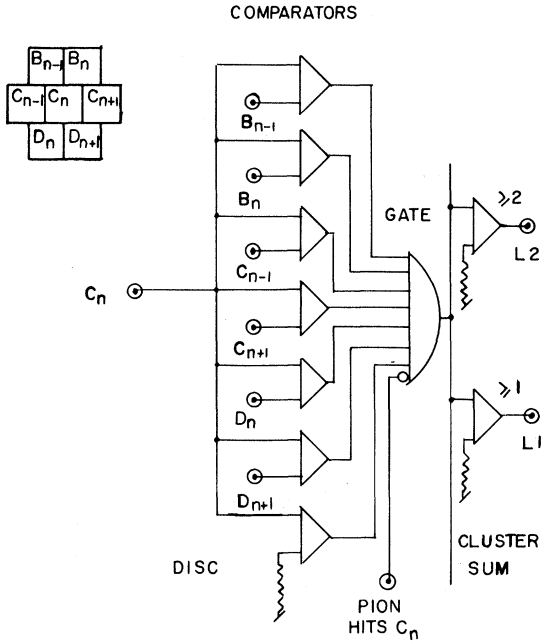

FIG. 3. Conceptual schematic of the γ-ray cluster logic. Differential fast comparators made of MC 10000 series integrated circuits were used to search the glass in parallel and find local maxima in pulse height. A voltage level proportional to the total number of such clusters was discriminated to generate outputs for at least one ($L1$) and at least two ($L2$). If the pion hodoscope H in front of the glass (Fig. 2) indicated that the observed local maximum was due to an incident charged particle, that maximum was vetoed.

line. Discriminators driven by the output line then gave a signal for the lower bound on the number of clusters. The whole process took about 50 nsec. The two outputs $L1$ (at least one cluster) and $L2$ (at least two clusters) were then used in the trigger logic.

The two scintillator-lead-scintillator sandwiches for γ-ray conversion before $M3$ are shown in Fig. 1(b). Veto counters $S4$ and $S6$ were placed in front of the lead, which was just ahead of MWPC $C3$. Coincidence counters $S5$ and $S7$ were just behind $C3$. The $\Lambda\to p\pi^-$ trigger signature was $T(\Lambda)=\overline{S1}\cdot C1\cdot C5N\cdot C6P\cdot S2$, where the C's refer to MWPC's in Fig. 1, $C5N$ is the negative-particle half of $C5$, and $C6P$ is the positive-particle half of $C6$. The signatures for two detected γ rays were $G2=\overline{S3}\cdot L2$ for two γ's in the glass, or $G1=\overline{S3}\cdot L1\cdot(\overline{S4}\cdot S5$ or $\overline{S6}\cdot S7)$ for one γ in the glass and one in $C3$. The complete Ξ^0 trigger was thus $T(\Xi)=T(\Lambda)\cdot(G1$ or $G2)$. Λ triggers without the γ-ray signature, predominantly $\Lambda\to p\pi^-$ from Λ's in the neutral beam, were reduced by a factor of $\frac{1}{128}$ by a prescaler and then mixed with the Ξ^0 triggers to supply a normalization for the Ξ^0 yield and to serve various calibration purposes. The signal [$T(\Xi)$ or $T(\Lambda)/128$] initiated the transfer of all the spectrometer MWPC coordinate data and the pulse heights for each lead-glass block to magnetic tape for off-line event reconstruction.

RESULTS

Data were taken at five production angles in the laboratory: 0, 2, 4, 7.5, and 10 mrad. About half of the total number of events came from the 7.5 mrad runs. A limited amount of data came from Ξ^0 production from copper (16%) and lead (15%) targets, but most of the results were from beryllium (69%). In the measurement of α_{Ξ^0} the three targets have been combined, and all of the production angles were used. The event reconstruction proceeded in three stages. First a pattern-recognition program used the coordinate information from the MWPC's to reconstruct a V topology and fit it to the hypothesis $\Lambda\to p\pi^-$. A laboratory coordinate system with z axis perpendicular to the chamber planes, x axis horizontal, and y axis vertical was established for this purpose. Second, Ξ^0 trigger events with an identified Λ were examined for two suitable γ-ray showers. A one-constraint fit was performed to the hypothesis $\Xi^0\to\Lambda\pi^0$, $\pi^0\to\gamma\gamma$ using the reconstructed Λ momentum, the positions but not the energies of the two γ-ray showers, forcing the π^0 mass, the Ξ^0 mass, and the Ξ^0 direction, and leaving the longitudinal coordinate of the Ξ^0-decay vertex as a variable parameter. The γ energies determined by this fit could be used to check the calibration of the lead-glass array, as mentioned above. Finally, events surviving the one-constraint fit were refit using the calibrated pulse-height information from the lead glass. This was a two-constraint fit for type $G1$ events and a three-constraint fit for type $G2$. Figure 4 shows the widths of the Ξ^0 invariant mass distributions for $G1$ and $G2$ events obtained by relaxing that constraint. The full width at half maximum of the $G1$ peak is about 18 MeV/c^2, while that of the $G2$ peak is 32 MeV/c^2. The $G1$ resolution appears better because one γ-ray energy had to be calculated for these events from the π^0 mass and the γ-γ opening angle: $E_2=m_\pi{}^2/\,2E_1(1-\cos\theta_{12})$; while for the $G2$ events two independently measured energies were used. The $G2$ Ξ^0 mass resolu-

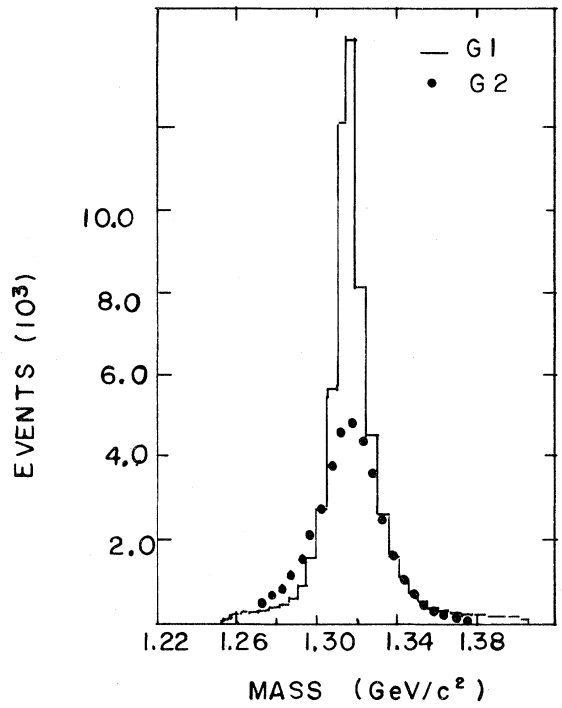

FIG. 4. Invariant mass of the $\Lambda\pi^0$ system for $G1$ and $G2$ Ξ^0 events calculated from $M_\Xi{}^2=m_\pi{}^2+m_\Lambda{}^2+2E_\Lambda(E_{\gamma1}+E_{\gamma2})-2\vec{p}_\Lambda\cdot(\vec{p}_{\gamma1}+\vec{p}_{\gamma2})$. Both $E_{\gamma1}$ and $E_{\gamma2}$ were independently measured in the lead glass for $G2$ events, while for $G1$ events $E_{\gamma2}$ had to be calculated from $E_{\gamma1}$ and π^0-decay kinematics, which resulted in a sharper resolution function. The bins are 5 MeV/c^2 wide.

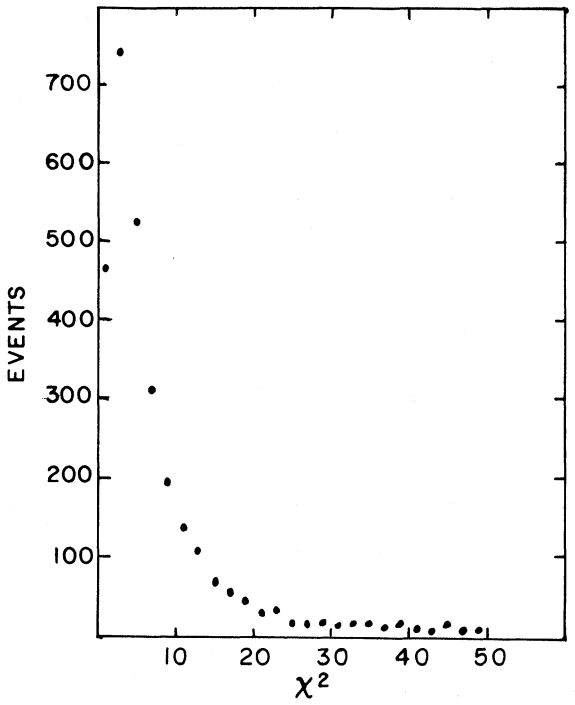

FIG. 5. Observed distribution in χ^2 for the $G2$ Ξ^0's, a three-constraint fit. Non-Gaussian errors in γ-ray energy and position shift the curve to higher $\langle\chi^2\rangle$ and make it broader than the classical χ^2 formula for three degrees of freedom. Events were accepted if $\chi^2 \leq 30$. The high-χ^2 tail has evidence of non-Ξ^0 background (see text).

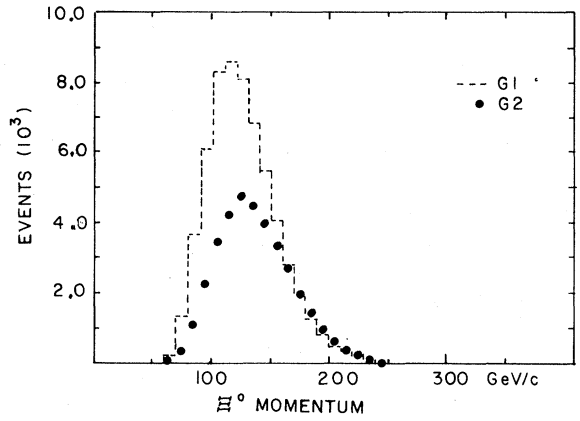

FIG. 6. Momentum distributions for fitted $G1$ and $G2$ Ξ^0's at 7.5 mrad production angle. The cutoff at low momenta is caused by the loss of Ξ^0's in the drift space between the target and the decay vacuum pipe (see Fig. 1). The high-momentum falloff is characteristic of the differential cross section for Ξ^0 production. The $G2$ Ξ^0's are shifted to slightly higher momenta than the $G1$'s because of the trigger requirement of two γ rays in the lead glass.

tion shown here is identical to the one reported in the earlier experiment.[4] A typical χ^2 distribution obtained for $G2$ events at 7.5 mrad production angle is shown in Fig. 5. The distribution is broader than that expected from the classical formula for χ^2 with three degrees of freedom. This is presumably due to the non-Gaussian errors associated with the γ-ray detection apparatus. There is a long tail at high χ^2 which contains non-Ξ^0 background, to be discussed below. The corresponding data for the $G1$ events is shifted towards a smaller value of $\langle\chi^2\rangle$, as is appropriate for a two-constraint fit, but is again broader than the χ^2 function. $G2$ events with $\chi^2 < 30$ and $G1$ events with $\chi^2 < 20$ were accepted into the final data sample. About 9% of the $G1$ and $G2$ triggers had satisfactory χ^2 for the Ξ^0 decay hypothesis. Figure 6 shows the momentum spectra of reconstructed $G1$ and $G2$ events at 7.5 mrad. The peaks are around 120 GeV/c, with the trigger slightly favoring higher momentum Ξ^0's in the $G2$ case.

Many kinematic distributions other than the $\Lambda\pi^0$ invariant mass served to verify that the χ^2 fit picked out Ξ^0 decays and rejected background. For example, Fig. 7 shows the distribution along the beam line of the vertices of Λ decays averaged over all momenta at 7.5 mrad production angle.

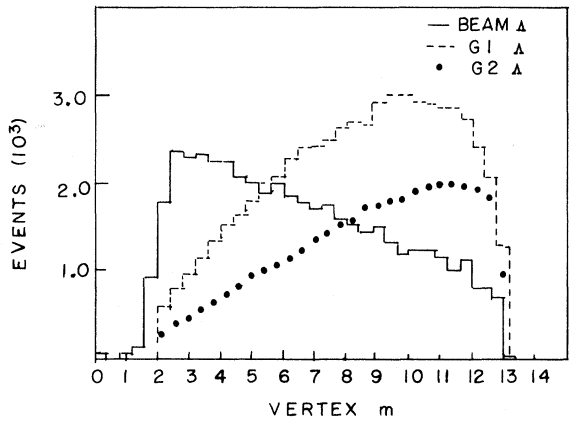

FIG. 7. Distributions of Λ vertices for 7.5-mrad production of Ξ^0 and Λ hyperons. These distributions have been integrated over Λ momentum: 60 GeV/$c \leq p_\Lambda \leq 240$ GeV/c, with an average value $\langle p_\Lambda \rangle \sim 100$ GeV/c. The beam Λ's show a roughly exponential decay curve beginning near the veto counter which defined the upstream limit of the Λ decay volume. In contrast, the daughter Λ's show a growth curve, beginning near the same veto counter and increasing going downstream. The detected Λ's have been reduced relative to the Ξ^0's by a factor of $\frac{1}{128}$ in the trigger.

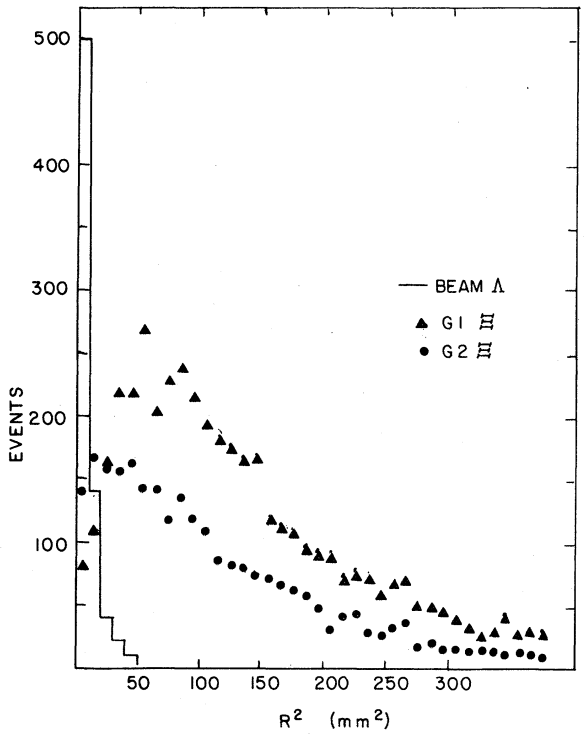

FIG. 8. Distributions of the square of the distance between the production target center and the Λ momentum vector extrapolated back to the target plane for beam Λ's and daughter Λ's from Ξ^0 decay. These data were taken at 7.5-mrad production angle, and have been averaged over p_Λ: 60 GeV/$c \leq p_\Lambda \leq$ 240 GeV/c. The actual target size was $R^2=9$ mm^2. The bins are 10 mm^2 wide. Note the sharp peak of the beam Λ's, characteristic of particles produced at the target, in contrast to the broad distribution of daughter Λ's which have acquired extra transverse momentum from the decay $\Xi^0\rightarrow\Lambda\pi^0$. The normalization of the Λ's relative to the Ξ^0's is arbitrary.

Daughter Λ's, that is those for which the $\Lambda\pi^0$ fit to a Ξ^0 was good, showed a characteristic growth curve as a function of distance, in contrast to the decay curve of the beam Λ's. Figure 8 shows another difference between beam and daughter Λ's—the "target pointing" variable distribution. This variable is the square of the distance in mm^2 between the center of the production target in the xy plane and the extrapolated intercept of the Λ momentum vector in that plane at the z coordinate of the target. Beam Λ's, which were made in the production target, pointed back to it, while daughter Λ's having acquired extra transverse momentum from the Ξ^0 decay, did not. The actual target radius was 3 mm. The $G1$ events were spread out to larger R^2 than the $G2$ events simply because of the definitions of the two topologies. A $G1$ event had one γ ray above or below the aperture of $M3$, which tended to give more transverse momentum to the π^0 and hence to the Λ. The $G2$ events were more tightly collimated.

Several cuts were applied to the final data sample in addition to the requirement of good χ^2 for the $\Xi^0\rightarrow\Lambda\pi^0$ decay hypothesis. All of the detected particles were required to hit the apparatus well within the appropriate active volumes. Each γ was required to have an energy greater than 3 GeV in the lead glass or greater than 1 GeV (computed from the fit) in $C3$. Coordinates of the γ rays on the glass were required to be 2 cm away from the borders of the array—neither near the hole nor near the outside edges. The Λ-decay vertex was required to be within the evacuated pipe, and the fitted Ξ^0 vertex was required to be downstream of the output face of $M2$.

The events in the high-χ^2 tail of the graph shown in Fig. 5 differ from the low-χ^2 events in their kinematic distributions, showing a broader mass plot than Fig. 4, a sharper R^2 distribution like the beam Λ's in Fig. 8, etc. Since the fit to $\Lambda\rightarrow p\pi^-$ was always good, the high χ^2 came from the combination of the Λ momentum vector with the two γ rays to form a Ξ^0. It was natural to assume that the two identified γ rays, either both in the lead glass or one in the lead glass and one in $C3$, were spurious, and were matched with a Λ decay in the neutral beam to form a poorly fitted Ξ^0. Real $\pi^0\rightarrow\gamma\gamma$ decays which were not associated with Ξ^0 decay could come from the neutral decay mode of another beam Λ, or from interactions in the small amount of material in the neutral beam (about 2% of an interaction length of carbon). Random hits from a variety of sources made up the rest of the two-γ background. It was believed that this background would be very difficult to model with Monte Carlo techniques. The final data sample was cut in χ^2 as described above, but the question remained: How many non-Ξ^0 events like those in the high-χ^2 tail happened to give a satisfactory fit to the Ξ^0-decay hypothesis and hence remained in the data after the cuts?

To answer this question the following approach was adopted. A sample of background γ-ray pairs was selected by taking all of the rejected Ξ^0-decay candidates, i.e., those $G1$'s with $\chi^2>20$ and those $G2$'s with $\chi^2>30$, and mixing the γ-ray hits from one event with the Λ decay from another. These uncorrelated (γ pair) + Λ's were then refit to the Ξ^0-decay hypothesis. The resulting χ^2 distributions

are shown in Figs. 9(a) and 9(b) for 7.5 mrad and in Fig. 11(a) and 11(b) for 0 mrad. The graphs show only about 10% of the total data, but the sample purity is typical. When normalized to the real data for all $\chi^2 \geq 60$, these fake events could be extrapolated to low χ^2 to estimate the non-Ξ^0-decay background. The results of this procedure are given in the captions to Figs. (10) and (12), where the real and fake events with good χ^2 are plotted as a function of the target pointing variable R^2. The contamination of the 7.5-mrad data (Fig. 10), where the Ξ^0/Λ ratio in the neutral beam was favorable (about 1 to 40), was $\sim 1\%$. The possible effects of this contamination on the final value of α_{Ξ^0} were ignored. As Figs. (11) and (12) show, the 0 mrad data had a larger background, 3% for $G1$ and 6% for $G2$. The Ξ^0/Λ ratio at 0 mrad was about 1 to 100. To eliminate effects due to this background the 0 and 2 mrad data were cut if $R^2 \leq 30$ mm^2, which left a contamination less than 1%. Thus the backgrounds decreased with increasing production angle, and were deemed negligible for 4, 7.5, and 10 mrad, while 0 and 2 mrad were cut on small R^2.

The final Ξ^0 data sample was analyzed to determine the direction of the spin of the daughter Λ through the asymmetry in the decay $\Lambda \rightarrow p\pi^-$. If time-reversal invariance is valid and final-state interactions are ignored,[5] the polarization is given in general by the expression

$$\vec{P}_\Lambda = \frac{(\alpha_\Xi + \hat{\Lambda}\cdot\vec{P}_\Xi)\hat{\Lambda} - \gamma_\Xi \hat{\Lambda}\times(\hat{\Lambda}\times\vec{P}_\Xi)}{1+\alpha_\Xi \hat{\Lambda}\cdot\vec{P}_\Xi}, \qquad (1)$$

where $\vec{P}_\Xi$ is the Ξ^0 polarization vector, and $\hat{\Lambda}$ is the direction of the Λ momentum in the Ξ^0 rest frame. The decay parameters satisfy the relation $\alpha_\Xi^2 + \gamma_\Xi^2 = 1$. Equation (1) shows that the spin

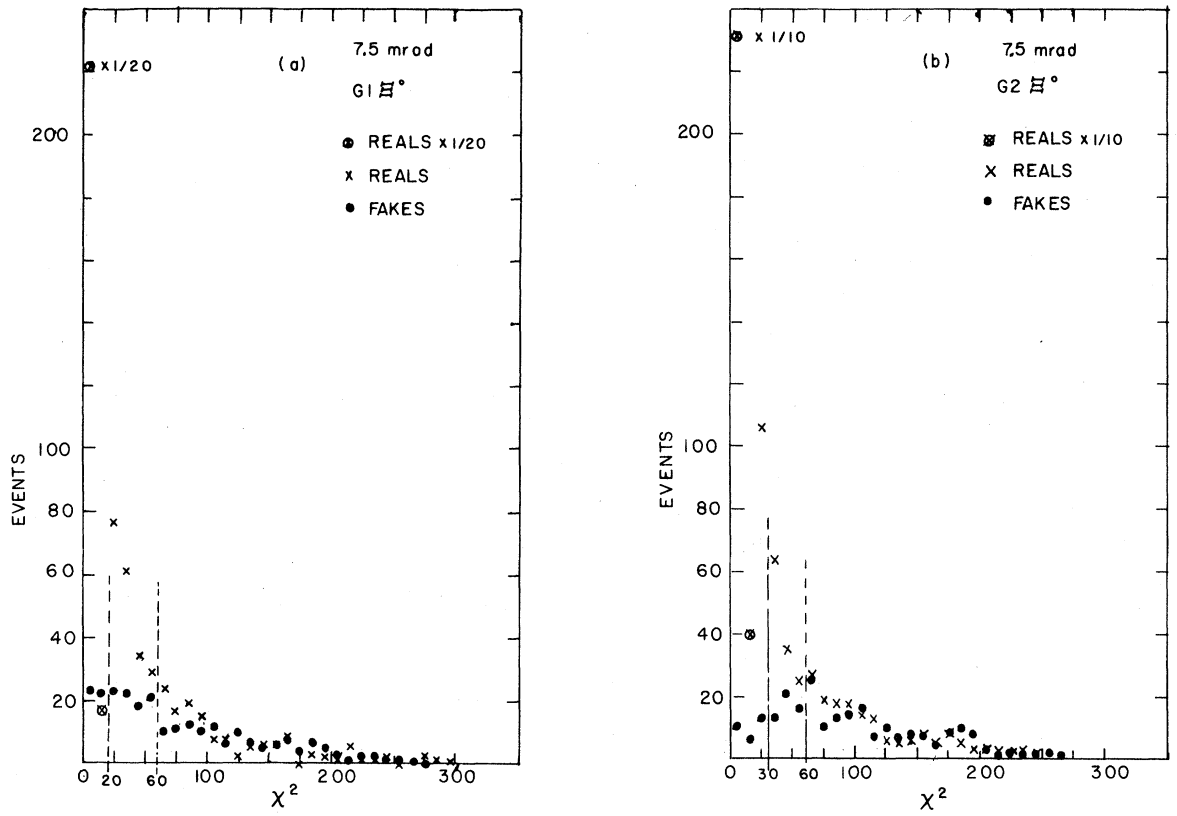

FIG. 9. χ^2 distributions for $G1$ and $G2$ Ξ^0 events at 7.5 mrad plotted (as crosses) to display the high-χ^2 tail. The data of (b) are plotted on an expanded scale in Fig. 5. Fake events were generated by taking those reconstructed Ξ^0s with $\chi^2 > 20$ for $1G$ and $\chi^2 > 30$ for $2G$ and mixing together uncorrelated Λ's and pairs of γ rays. The χ^2 distributions obtained by this method and normalized to the real events for $\chi^2 \geq 60$ are also plotted (as circles). The ratios of the circles to the crosses for $\chi^2 < 20$ [(a)] and $\chi^2 < 30$ [(b)] have been taken as a measure of the non-Ξ^0 background in the data sample.

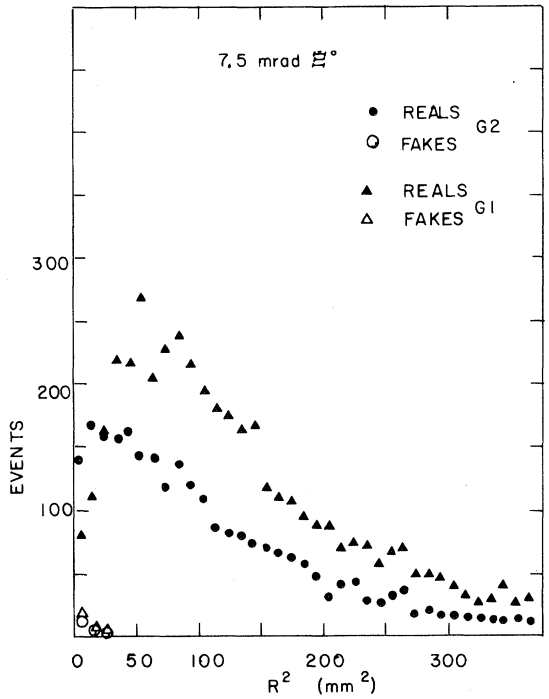

FIG. 10. Real and fake events from Fig. 9(a) cut at $\chi^2 \leq 20$ and plotted as closed and open triangles, respectively, and real and fake events from Fig. 9(b) cut at $\chi^2 \leq 30$ and plotted as closed and open circles. The real data are identical to those shown in Fig. 8. The small peaks formed by the fake events resemble the beam Λ peak in Fig. 8, and represent the estimate of the non-Ξ^0 background in the final data samples. For the data shown the numbers are 44 fake events and 4793 reals for $G1$ and 29 fake events and 2734 reals of $G2$. No corrections were made to α_{Ξ^0} for these possible backgrounds.

direction of the daughter Λ depends both on the decay asymmetry parameter α_Ξ of the parent and on the Ξ^0 polarization. The spin direction could be determined by measuring the proton-decay asymmetry in the Λ rest frame through the relation

$$\frac{dN}{d\Omega} = \frac{1}{4\pi}(1+\alpha_\Lambda \vec{P}_\Lambda \cdot \hat{p}) , \qquad (2)$$

where $\hat{p}$ is a unit vector along the daughter-proton direction in the Λ rest frame and $\vec{P}_\Lambda$ is given by Eq. (1). (In order to be relativistically correct, the proton direction in the Λ rest frame in Eq. (2) should be obtained by transforming the proton from the laboratory to the Ξ^0 rest frame and then to the Λ rest frame, and this was done in the analysis, although the difference between this procedure and a direct Lorentz transformation from

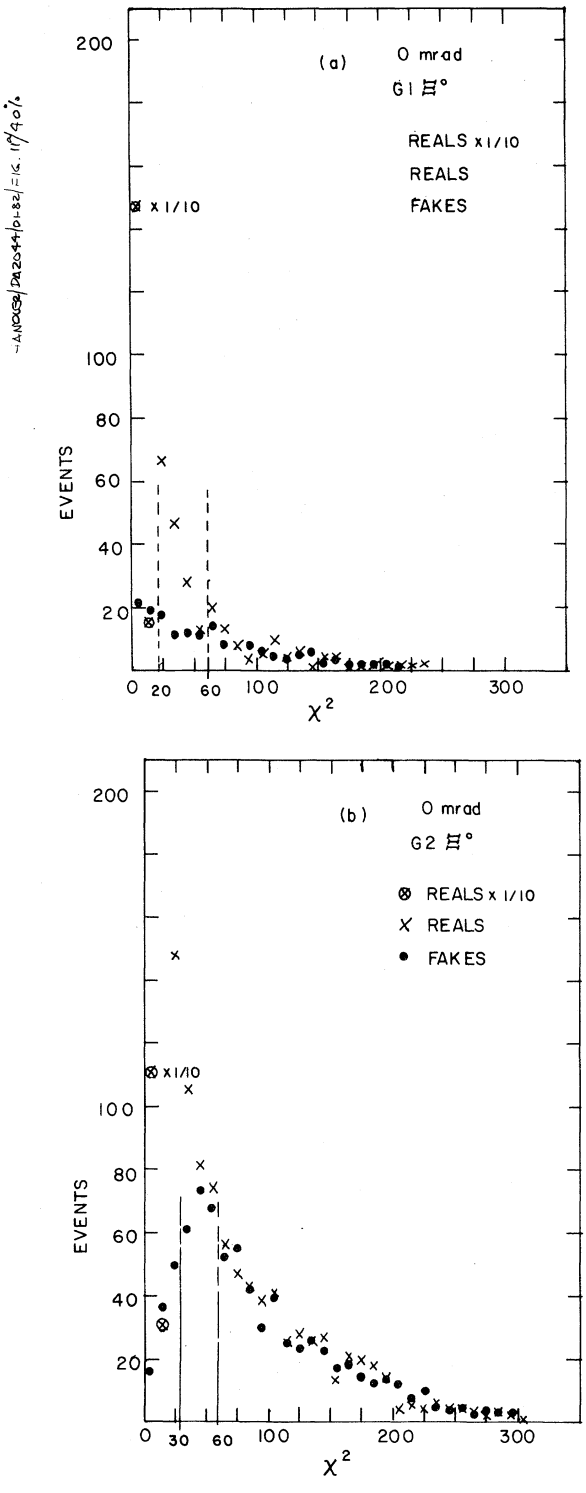

FIG. 11. Graphs (a) and (b) identical to Figs. 9(a) and 9(b) except at 0 mrad production angle, where the ratio of Ξ^0/Λ in the neutral beam was smaller, and backgrounds were expected to be larger. The normalization of fake events to real events was the same as described for Fig. 9.

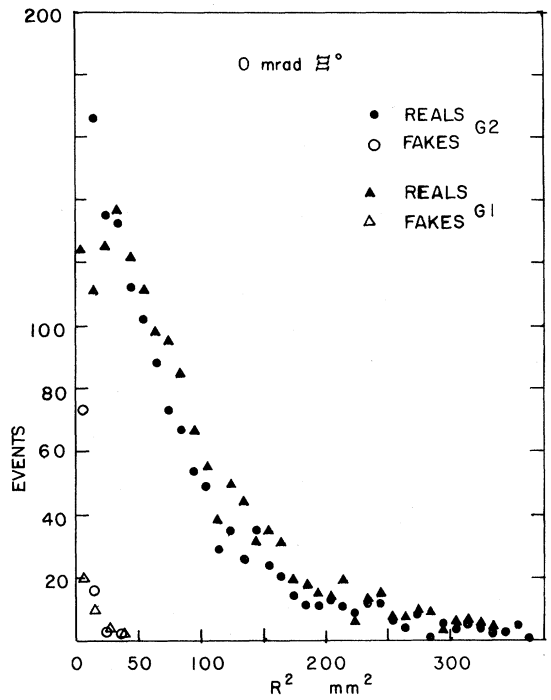

FIG 12. The same plot as Fig. 10 except for 0 mrad. The numbers are 41 fake events and 1633 real events for $G1$ and 102 fake events and 1575 real events for $G2$. After a cut requiring $R^2 \geq 30$ mm^2, applied to both the 0 and 2 mrad data, the remaining backgrounds were $\sim 0.5\%$ and were neglected.

the laboratory to the Λ rest frame was at most a few degrees because of the low velocities of the baryon daughters in the decay chain.) In this way all of the information about the Ξ^0 polarization, its magnetic moment,[6] and the asymmetry parameter α_Ξ were obtained from Λ decay, without the need to refer to asymmetries or distributions in the rest frame of the Ξ^0. This proved to be of great utility, because extensive experience has been gained in measuring Λ polarization with this apparatus,[7,8] which had excellent acceptance for Λ decays, and well understood distortions of the daughter-proton distribution functions projected on the three laboratory axes (x,y,z) defined earlier. The proton asymmetry distribution along a fixed direction, $\hat{x}$ for instance, $dN/d\cos\theta_x = (1+A_x\,\hat{p}\cdot\hat{x})/2$, was measured using the hybrid Monte Carlo technique described by Bunce in Ref. 8. For each real event ten accepted Monte Carlo events were generated with all parameters except $\cos\theta_x$ fixed, and $\cos\theta_x$ varying from -1 to $+1$. A χ^2 technique gave the best value for the asymmetry parameter A_x which appeared both in the real data and the Monte Carlo, and also gave a goodness-of-fit test in the minimum value of χ^2 obtained.

The relation between $\vec{P}_\Lambda$ and the observables α_Ξ, γ_Ξ, and $\vec{P}_\Xi$ displayed in Eq. (1) is complicated. There are several unknowns, they appear in the denominator as well as the numerator, and they are correlated with the unit vector $\hat{\Lambda}$ which varied from event to event rather than being fixed in space. An effect called the "bias" added to the confusion. The hybrid Monte Carlo failed to reproduce the acceptance of the apparatus precisely for Λ momenta below about 140 GeV/c,[9] which led to a false polarization asymmetry called $\vec{B}_\Lambda$, a vector dependent on the Λ momentum but otherwise constant and fixed in space. Thus the observed Λ polarization could be written.

$$(\vec{P}_\Lambda)_{\text{observed}} = (\vec{P}_\Lambda)_{\text{true}} + \vec{B}_\Lambda \,, \tag{3}$$

where $(\vec{P}_\Lambda)_{\text{true}}$ is given by Eq. (1). The bias increased the number of quantities which had to be measured in the experiment. Data were taken under enough different conditions to allow the independent determination of α_Ξ, $\gamma_\Xi\vec{P}_\Xi$, and $\vec{B}_\Lambda$. The polarization $\vec{P}_\Xi = 0$ at 0 mrad production, and at any nonzero angle the sense of $\vec{P}_\Xi$ could be reversed by rotating the Ξ^0 production plane by 180°. This rotation was accomplished by reflecting the incident proton beam vector $\vec{k}_{\text{in}}$ in the horizontal plane, so that the normal to the production plane $\hat{n} = \vec{k}_{\text{in}} \times \vec{k}_{\text{out}} / |\vec{k}_{\text{in}} \times \vec{k}_{\text{out}}|$ pointed either along $+\hat{x}$ or $-\hat{x}$. At each production angle θ half of the data was taken with n parallel to $+\hat{x}$ (positive θ) and half with n parallel to $-\hat{x}$ (negative θ). The combined sample had $\vec{P}_\Xi = 0$ at each angle for a given excitation of the precession magnet $M2$. Adding the observed asymmetries for $+\theta$ and $-\theta$ isolated $\alpha_\Xi\hat{\Lambda}$ and $\vec{B}_\Lambda$ terms in $\vec{P}_\Lambda$, cancelling out effects due to $\vec{P}_\Xi$, while subtracting the asymmetries had the opposite effect.

An iterative procedure was adopted to measure the quantities α_Ξ, which was a constant under all conditions, $\vec{P}_\Xi$, which depended on production angle, Ξ^0 momentum, and $M2$ excitation, and $\vec{B}_\Lambda$, which depended only on momentum. A first value of α_Ξ was obtained from the 0 mrad data, where $\vec{P}_{\Xi^0} = 0$, by taking only those Λ momenta for which $\vec{B}_\Lambda \approx 0$ as well, leaving $\vec{P}_\Lambda = \alpha_\Xi\hat{\Lambda}$. This initial value, $(\alpha_\Xi\alpha_\Lambda)_1$, could then be substituted into the full expression for $\vec{P}_\Lambda$ at 7.5 mrad, where $\vec{P}_\Xi \neq 0$. A power-series expansion of the denominator was used:

$$\vec{P}_\Lambda=\alpha_\Xi\hat{\Lambda}+(1-\gamma_\Xi)(\vec{P}_\Xi\cdot\hat{\Lambda})\hat{\Lambda}+\gamma_\Xi\vec{P}_\Xi-\alpha_\Xi^2(\vec{P}_\Xi\cdot\hat{\Lambda})\hat{\Lambda}-\alpha_\Xi(1-\gamma_\Xi)(\vec{P}_\Xi\cdot\hat{\Lambda})^2\hat{\Lambda}$$
$$-\alpha_\Xi\gamma_\Xi(\hat{\Lambda}\cdot\vec{P}_\Xi)\vec{P}_\Xi+\alpha_\Xi^3(\hat{\Lambda}\cdot\vec{P}_\Xi)^2\hat{\Lambda}+\cdots+\vec{B}_\Lambda\,. \tag{4}$$

By subtracting the $+7.5$ mrad (normal to the production plane along $+\hat{x}$) asymmetry from the -7.5 mrad asymmetry, the effect due to α_Ξ, $\vec{B}_\Lambda$, and terms quadratic in $\vec{P}_\Xi$ canceled out, leaving $(\vec{P}_\Xi)_1$ as a result. The sum of the $+7.5$ mrad and -7.5 mrad data, together with the trial values of $(\alpha_\Xi)_1$ and $(\vec{P}_\Xi)_1$ then gave the bias vector $(\vec{B}_\Lambda)_1$. $(\vec{P}_\Xi)_1$ and $(\vec{B}_\Lambda)_1$ were then used to obtain $(\alpha_\Xi)_2$, etc. The process quickly converged to stable values of the unknowns which best fit the data. The results were consistent with a bias vector $\vec{B}_\Lambda$ which was a function only of momentum, independent of production angle.

The analysis had to keep track of many different categories of data: (a) $G1$ and $G2$ Ξ^0's; (b) six different excitations of the magnet $M2$ which precessed the Ξ^0 magnetic moment; (c) five different production angles, with each sign for ±2, ±4, ±7.5, and ±10 mrad; (d) three different Ξ^0 production targets, beryllium, copper, and lead; (e) six different momentum bins for the Ξ^0's, 0–120, 120–140, 140–160, 160–180, 180–200, and 200–400 GeV/c. For the purpose of the present discussion the data have been combined for various values of $M2$ excitation, production angle sign, and production target. Table I gives the breakdown of the numbers of events at the various angles and the fractions taken with the three metal targets. Figure 13 shows the Ξ^0 polarization at 7.5 mrad for the $G1$ and $G2$ samples combined. Figure 14 shows the components of the bias vector $\vec{B}_\Lambda$ averaged over $G1$ and $G2$ for the three angles 4, 7.5, and 10 mrad. The polarization depended on production angle, of course, while the bias, as mentioned earlier, was angle independent within the errors. The small magnitude of the Ξ^0 polarization ($\langle|P_\Xi|\rangle=0.10$) assured the rapid convergence of the expansion in Eq. (4). The general trend in the bias as a function Ξ^0 momentum agrees well with polarization biases previously observed in this apparatus and reported in Ref. 9. The large value of $B_{\Lambda z}$ in the lowest momentum bin was presumed to be caused by a loss in acceptance of the apparatus at low momenta which was not correctly modeled by the hybrid Monte Carlo. The dynamics of the Ξ^0 polarization will be discussed in a separate article.

The value of α_Ξ obtained by the iterative fit outlined above should not be affected by the bias or the polarization, since the data were used to obtain best numbers for all of the unknowns. Table II shows the results for $\alpha_\Lambda\alpha_\Xi$ as a function of momentum averaged over all angles for $G1$ and $G2$ separately, $G1$ and $G2$ combined, and finally all momenta combined, to give the result $\alpha_\Lambda\alpha_\Xi=-0.260\pm0.004$, where the error is statistical only. The individual errors were obtained from the χ^2 fits to the asymmetries (Ref. 8) and did not always precisely track with the number of events. The averaged values as a function of Ξ^0 momentum are plotted in Fig. 15. As can be seen from the numbers, all of the values for $\alpha_\Lambda\alpha_\Xi$ are internally consistent with each other. A systematic error of 0.005 was added in quadrature with the statistical error to cover possible background effects in the data example. The final result is

$$\alpha_\Lambda\alpha_\Xi=-0.260\pm0.006\,.$$

TABLE I. Data Sample Used to Measure $\alpha_\Lambda\alpha_{\Xi^0}$.

Production angle (mrad)	Events $G1$	Events $G2$	Fraction of data from each production target Be	Cu	Pb
0	11346	9411	40%	30%	30%
2	5669	3823	26%	36%	38%
4	28305	22377	53%	22%	25%
7.5	93887	58051	83%	8%	9%
10	45395	23843	63%	21%	16%
total	184602	117505	69%	16%	15%

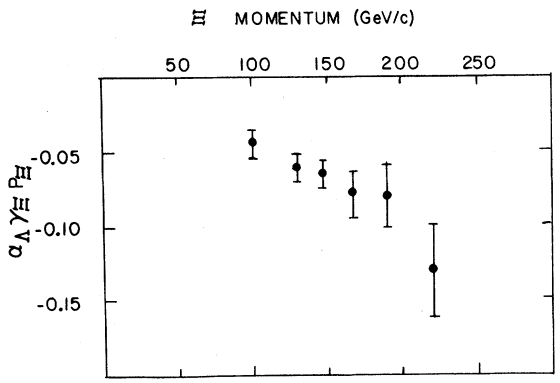

FIG. 13. Ξ^0 polarization as a function of Ξ^0 momentum at 7.5 mrad production angle. The quantity plotted is $\alpha_\Lambda \gamma_\Xi P_\Xi$, which is the asymmetry actually measured in the experiment. Since γ_Ξ is positive, the term $\gamma_\Xi \vec{P}_\Xi$ dominates in Eq. (4) for $\vec{P}_\Lambda$, and the proton asymmetry in Λ decay is decreased by the extra factor α_Λ. The polarization was defined to be positive along the direction $\hat{n} = \vec{k}_{in} \times \vec{k}_{out} / |\vec{k}_{in} \times \vec{k}_{out}|$ where $\vec{k}_{in}$ was the incident proton beam direction and $\vec{k}_{out}$ was the direction of the produced Ξ^0 hyperon. This vector was parallel to $+\hat{x}$ for positive production angles. The quantity plotted here was obtained by subtracting the -7.5 mrad asymmetry from the $+7.5$ mrad asymmetry. Although averaged over target materials, this result was predominantly from beryllium (see Table I).

This result differs by two standard deviations from the result of Ref. (4): $\alpha_\Lambda \alpha_{\Xi^0} = -0.317 \pm 0.027$. The difference is not inconsistent with a statistical fluctuation, although the present experiment had more data, better acceptance, and less background than its predecessor. Dividing by the world aver-

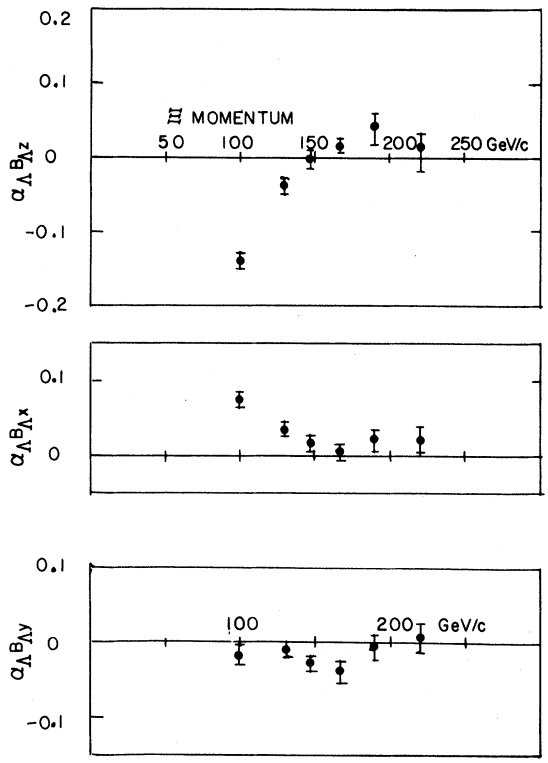

FIG. 14. The three components of the bias vector defined by Eq. (3) multiplied by α_Λ and plotted as a function of Ξ^0 momentum in the laboratory coordinate system shown in Figs. 1(a) and 1(b). The average momentum of daughter Λ's was about 85% of that of the parent Ξ^0, so that in terms of p_Λ the lowest point is at 85 GeV/c. The z and y biases closely follow the results obtained by Schachinger in Ref. 9. The low-momentum x biases plotted here are somewhat larger than those of Ref. (9).

TABLE II. Results for $\alpha_\Lambda \alpha_{\Xi^0}$.

Ξ^0 momentum bins (GeV/c)	Average Ξ^0 momentum (GeV/c)	Averaged over all production angles Type $G1$ Events	$\alpha_\Lambda \alpha_\Xi$	Type $G2$ Events	$\alpha_\Lambda \alpha_\Xi$	$G1$ and $G2$ averaged Events	$\alpha_\Lambda \alpha_\Xi$
0–120	102	82 561	-0.260 ± 0.010	33 867	-0.266 ± 0.015	116 428	-0.262 ± 0.008
120–140	130	43 018	-0.265 ± 0.010	26 349	-0.255 ± 0.013	69 367	-0.261 ± 0.008
140–160	150	28 408	-0.268 ± 0.012	21 955	-0.270 ± 0.014	50 363	-0.269 ± 0.009
160–180	169	15 711	-0.234 ± 0.016	15 518	-0.272 ± 0.017	31 229	-0.253 ± 0.011
180–200	189	8 010	-0.226 ± 0.023	9 462	-0.265 ± 0.021	17 472	-0.247 ± 0.015
200–400	227	6 894	-0.218 ± 0.026	10 354	-0.255 ± 0.021	17 248	-0.241 ± 0.016
Grand averages		184 602	-0.256 ± 0.005	117 505	-0.264 ± 0.006	302 107	-0.260 ± 0.004

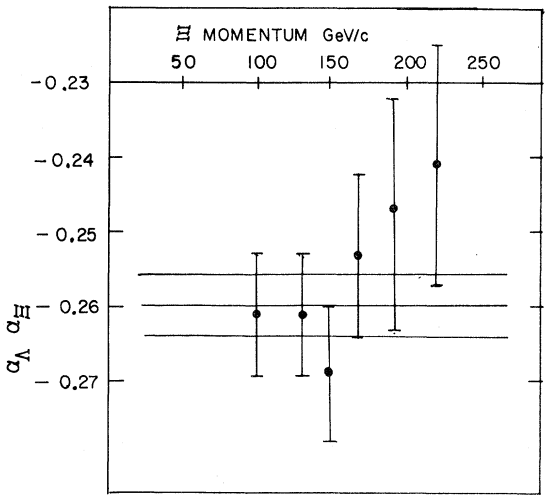

FIG. 15. Results for $\alpha_\Lambda\alpha_\Xi$ as a function of Ξ^0 momentum averaged over all production angles with $G1$ and $G2$ samples combined. Note the suppressed zero on the ordinate axis. The grand average and statistical errors are shown on parallel lines.

age of $\alpha_\Lambda = 0.642 \pm 0.013$ (Ref. 10) yields $\alpha_{\Xi^0} = -0.405 \pm 0.012$, where the uncertainty comes equally from this measurement and the world average of α_Λ. The previous world average was $\alpha_{\Xi^0} = -0.47 \pm 0.05$ (Refs. 4,11) and the new average is $\alpha_{\Xi^0} = -0.407 \pm 0.012$.

CONCLUSIONS

The daughter-baryon polarization in the decay $B \to B'\pi$, given by Eq. (1), depends on the parameters α and γ, which in turn are functions of the S-wave (parity-violating) and P-wave (parity-conserving) amplitudes which give a phenomenological description of the $j = \frac{1}{2} \to j = \frac{1}{2}$ decay. If the final-state $\Lambda\pi$ phase shifts are suppressed and time-reversal invariance is assumed, the relations are as follows: the rate $\Gamma = S^2 + P^2$, the asymmetry parameter $\alpha = 2SP/\Gamma$, and the parameter $\gamma = (S^2 - P^2)/\Gamma$.[5] Equivalent dimensionless amplitudes A and B have been used by Overseth.[12] A phenomenological decay amplitude for the process $B \to B'\pi$ is written as $\mathcal{M} = G_F m_\pi{}^2 [\bar{u}(p_2)(A + B\gamma_5) u(p_1)]$, where p_1 is the four-momentum of the parent hyperon with mass M, and p_2 is the four-momentum of the daughter with mass m. The dimensionless product $G_F m_\pi{}^2 = 2.213 \times 10^{-7}$. If the daughter meson has mass μ, then the ratio of P-wave to S-wave amplitudes is given by

$$P/S = \{[(M-m)^2 - \mu^2]/[(M+m)^2 - \mu^2]\}^{1/2} B/A = CB/A \ ,$$

and the decay rate is given by

$$\Gamma = G_F{}^2 m_\pi{}^4 (q/8\pi)(\{[(M+m)^2 - \mu^2]/M^2\} A^2 + \{[(M-m)^2 - \mu^2]/M^2\} B^2) \ .$$

Here q is the magnitude of the three-momentum in the decay. The $\Xi^0 \to \Lambda\pi^0$ decay rate is insensitive to the B amplitude, and hence determines A^2. The asymmetry parameter α gives two roots for the ratio B/A: $B/A = [1 \pm (1-\alpha^2)]^{1/2}/\alpha C$, where C is the mass factor defined above. The choice of root is determined by the sign of the decay parameter γ. The decay rate and the sign of γ_Ξ have been measured in other experiments.[11,13] Combining these results with the new world average for α_{Ξ^0} gives $A = 1.55 \pm 0.03$ and $B = -5.46 + -0.18$. These amplitudes, together with the corresponding ones for the decays of other hyperons, should be calculable from QCD corrections to the standard theory of weak interactions.

The test of the $|\Delta\vec{I}| = \frac{1}{2}$ rule in $\Xi \to \Lambda\pi$ decays presented by Overseth[12] is altered slightly by the new measurement of α_{Ξ^0}. In the notation of Ref. 12, $\Delta\alpha =$ measured α_0/α_- minus the predicted value, with the same definition for $\Delta\Gamma$. To first order in the ratios of $|\Delta\vec{I}| = \frac{3}{2}$ amplitudes to $|\Delta\vec{I}| = \frac{1}{2}$ amplitudes the numerical formulas are $\Delta\alpha = 1.37\,(A_3/A_1 - B_3/B_1)$ and $\Delta\Gamma = -1.44\,(A_3/A_1) - 0.06(B_3/B_1)$. The new value for $\Delta\alpha = 0.010 \pm 0.049$, while $\Delta\Gamma = 0.066 \pm 0.020$ remains the same. The new amplitude ratios then are $(A_3/A_1) = -0.041 \pm 0.013$ and $(B_3/B_1) = -0.051 \pm 0.036$, compared to -0.038 ± 0.014 and -0.17 ± 0.09, respectively, in Ref. 12. The A ratio is determined predominantly by the 3σ effect in $\Delta\Gamma$ and remains essentially unchanged, while the B ratio has decreased both in value and error by about a factor of 3. Further improvements in the precision of $\Delta\alpha$ will not change the A ratio, but the B ratio will approach the A ratio, since $A_3/A_1 = B_3/B_1$ if $\Delta\alpha = 0$. A more precise value for the lifetime of the Ξ^0 is needed to further test the statistical significance of these results. The present numbers are of the same order as various I-spin-violating effects such as mass differences and radiative corrections.

ACKNOWLEDGMENTS

We gratefully acknowledge the help of the staff of Fermilab, in particular that of the Meson Labo-

ratory, during the running of this experiment. Much of the apparatus was designed and built by E. Behr, S. Fraser, A. Jaske, and G. Ott. D. Mills assisted with the data taking. This research was supported in part by the United States Department of Energy and in part by the National Science Foundation.

---

[1]S. Weinberg, Phys. Rev. Lett. 19, 1264 (1967); A. Salam, in *Elementary Particle Theory: Relativistic Groups and Analyticity (Nobel Symposium No. 8)*, edited by N. Svartholm (Almqvist and Wiksell, Stockholm, 1968), p. 367.

[2]J. Finjord and M. K. Gaillard, Phys. Rev. D 22, 778 (1980), and references therein.

[3]P. Skubic *et al.*, Phys. Rev. D 18, 3115 (1978).

[4]G. Bunce *et al.*, Phys. Rev. D 18, 633 (1978).

[5]This discussion assumes that the angle $\phi=0°$, where $\tan\phi=\beta/\gamma$. The world average of experimental values is $\phi=20.7°\pm11.7°$. [See Particle Data Group, Rev. Mod. Phys. 52, S1 (1980).] A value of ϕ as large as 20° is probably not realistic, but would affect the present experimental value for α_Ξ by about 1 standard deviation. The argument is as follows. A value $\phi=20°$ would decrease the magnitude of γ by 6%, which would increase the magnitude of P_Ξ by the same amount, since the experiment measures the product $\gamma_\Xi\vec{P}_\Xi$ to first order. Equation (4) shows that the major correction to $\alpha_\Xi\hat{\Lambda}$ is $\alpha_\Xi^2(\hat{\Lambda}\cdot\vec{P}_\Xi)\hat{\Lambda}$, giving $\Delta\alpha\sim\alpha_\Xi\Delta P_\Xi\sim2.5\%$. Since α_Ξ is negative, an increase in $|P_\Xi|$ would result in an increase in $|\alpha_\Xi|$.

[6]P. T. Cox *et al.*, Phys. Rev. Lett. 46, 877 (1981).

[7]L. Schachinger *et al.*, Phys. Rev. Lett. 41, 1348 (1978).

[8]G. Bunce, Nucl. Instrum. Methods 172, 553 (1980).

[9]L. C. Schachinger, Ph.D. Thesis, Rutgers University, 1978 (unpublished).

[10]O. E. Overseth and R. F. Roth, Phys. Rev. Lett. 19, 391 (1967); W. Cleland *et al.*, Nucl. Phys. B40, 221 (1972); P. Astbury *et al.*, *ibid.* B99, 30 (1975).

[11]The same experiment has served to measure τ_{Ξ^0}, α_{Ξ^0}, and γ_{Ξ^0} in several instances. The most recent is that of C. Baltay *et al.*, Phys. Rev. D 9, 49 (1974).

[12]O. E. Overseth, in Particle Data Group, Rev. Mod. Phys. 52, S277 (1980).

[13]The world average for $\tau_{\Xi^0}=(2.90\pm0.10)\times10^{-10}$ sec, with a branching ratio $\Xi^0\to\Lambda\pi^0>99\%$. The most recent measurement is that of G. Zech *et al.*, Nucl. Phys. B 124, 413 (1977).